Peer-reviewed version available at Sensors 2018, 18, 1236; doi:10.3390/s18041236

Article

A Closed-Form Error Model of Straight Lines for Improved Data Association and Sensor Fusing

Volker Sommer [1,†*]

[1] Beuth University of Applied Sciences; sommer@beuth-hochschule.de
† Current address: Luxemburger Str. 10, D-13353 Berlin

Abstract: Linear regression is a basic tool in mobile robotics, since it enables accurate estimation of straight lines from range-bearing scans or in digital images, which is a prerequisite for reliable data association and sensor fusing in the context of feature-based SLAM. This paper discusses, extends and compares existing algorithms for line fitting applicable also in case of strong covariances between the coordinates at each single data point, which must not be neglected if range-bearing sensors are used. Besides, particularly the determination of the covariance matrix is considered, which is required for stochastic modeling. The main contribution is a new error model of straight lines in closed form for calculating fast and reliably the covariance matrix dependent on just a few comprehensible and easily obtainable parameters. The model can be applied widely in any case when a line is fitted from a number of distinct points also without a-priori knowledge of the specific measurement noise. By means of extensive simulations the performance and robustness of the new model in comparison to existing approaches is shown.

Keywords: linear regression; covariance matrix; data association; sensor fusing; SLAM

1. Introduction

Contour points acquired by active sensors using sonar, radar or lidar [1], or extracted from image data [2][3], are a key source of information for mobile robots in order to detect obstacles or to localize themselves in known or unknown environment [4][5]. For this purpose, often geometric features are extracted from raw data since in contrast to detailed contours, features are uniquely described just by a limited set of parameters and their extraction works as additional filtering in order to improve reliability when dealing with sensor noise and masking [6]. However, the performance of feature based localization or SLAM strongly depends on exact determination of a feature vector $\underline{y}$ from measured raw data. Moreover, especially for data association as well as for sensor fusing not only the feature parameters are needed, but also a reliable estimation of their covariance matrix $\underline{R}$ is required, which encapsulates the variances of the single elements in $\underline{y}$ and their dependencies.

This will be obvious if one looks at the standard algorithm for updating an estimated system state $\underline{\hat{x}}$ typically by means of EKF, compare [7][8][9]: New measurements $\underline{y}$ are plausible if their deviations from expected measurements $\underline{\hat{y}} = \underline{h}(\underline{\hat{x}})$ dependent on the in general non-linear measurement model $\underline{h}(\underline{\hat{x}})$ is within a limited range. For exact calculation of this limit usually the *Mahalanobis*-metric is applied, see [8][10], which considers the covariance matrix $\underline{S}$ of the innovation $\underline{\nu} = \underline{y} - \underline{\hat{y}}$ with $\underline{S} = \underline{R} + \underline{H} \cdot \underline{\hat{P}} \cdot \underline{H}^T$ dependent on $\underline{R}$, the covariance matrix $\underline{\hat{P}}$ of the system state and using $\underline{H} = \nabla \underline{h}(\underline{\hat{x}})$. A new measurement $\underline{y}$ will be considered to relate to an already known feature vector $\underline{\hat{y}}$ if its distance is below a given threshold r_{th} with $\underline{\nu}^T \underline{S}^{-1} \underline{\nu} < r_{th}^2$. Only in this case, the system state vector $\underline{\hat{x}}$ can be updated by means of $\Delta\underline{\hat{x}} = \underline{K} \cdot \underline{\nu}$ using the Kalman-gain $\underline{K} = \underline{\hat{P}} \cdot \underline{H}^T \cdot \underline{S}$, again depending on the covariance matrix $\underline{R}$ of the measurements, while otherwise $\underline{\hat{x}}$ and $\underline{\hat{P}}$ are expanded by the new feature.

Particularly in artificial environments straight lines in a plane are frequently used as features, since these are defined by just two parameters and can be clearly and uniquely determined. In contrast to point features, lines in images are almost independent of illumination and perspective, and a number

Preprints (www.preprints.org) | NOT PEER-REVIEWED | Posted: 13 March 2018 doi:10.20944/preprints201803.0093.v1

Peer-reviewed version available at Sensors 2018, 18, 1236; doi:10.3390/s18041236

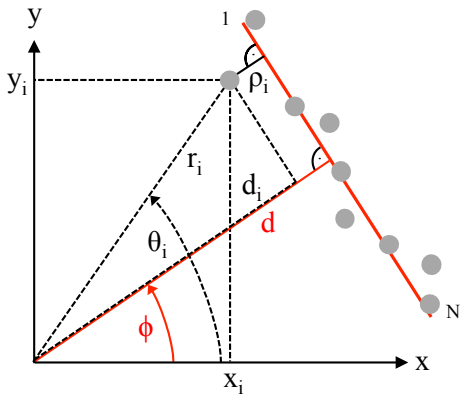

Figure 1. Parameters of measured raw data and fitted straight line

of measurements can be taken along their length to localise them accurately and to distinguish them from artifacts [11]. Moreover, already a single line enables a robot to determine its orientation and perpendicular distance, which clearly improves localization accuracy. Thus, many tracking systems have been proposed based on line features, either using range-bearing scans [12][13] or applying visual servoing, see [14][15], and also recently this approach has been successfully implemented [16][17][18]. However, due to missing knowledge of the covariance matrix, for data association often suboptimal solutions like the Euclidian distance in Hough space [12] or other heuristics are used [19].

Obviously, fitting data to a straight line is a well-known technique, addressed in a large number of papers [20][21][22] and textbooks [23][24][25]. In [26], a recent overview of algorithms in this field is outlined. As shown in [27] and [28], if linear regression is applied to data with uncertainties in x- and y-direction, always both coordinates must be considered as random variables. In [29], Arras and Siegwart suggest an error model for range-bearing sensors including a covariance matrix, affected exclusively by noise in radial direction. Pfister et al. introduce weights into the regression algorithm in order to determine the planar displacement of a robot from range bearing scans [30]. In [31], a maximum likelihood approach is used to formulate a general strategy for estimating the best fitted line from a set of non-uniformly weighted range measurements. Also merging of lines and approximating the covariance matrix from an iterative approach is considered. In [27] Krystek and Anton point out that the weighting factors of the single measurements depend on the orientation of a line, which therefore can only be determined numerically. This concept has been later extended to the general case with covariances existing between the coordinates of each data point [32].

Since linear regression is sensitive with respect to outliers, split-and-merge algorithms must be applied in advance, if a contour consists of several parts, see [33,34]. In cases of strong interference, straight lines can still be identified by Hough-transformation, compare [35–37], or alternatively RANSAC algorithms can be applied, see [38,39]. Although these algorithms work reliably, exact determination of line parameters and estimating their uncertainties still requires linear regression [40].

In spite of a variety of contributions in this field, there is missing a straightforward but yet accurate algorithm for determining the covariance matrix of lines reliably, fast and independently of the a-priori mostly unknown measurement noise. In chapter 4 such a model in closed-form is proposed depending on just a few clearly interpretable and easily obtainable parameters. Beforehand, in the next two paragraphs existing methods for linear regression and calculation of the covariance matrix are reviewed with certain extensions focussing on the usage of range-bearing sensors, which cause strong covariances between x- and y-coordinates. Based on these theoretical foundations paragraph 5 exhibits detailed simulation results in order to compare precision and robustness of the presented algorithms.

Peer-reviewed version available at Sensors 2018, 18, 1236; doi:10.3390/s18041236

2. Determination of accurate line parameters

In 2d-space each straight line is uniquely described by its perpendicular distance d from origin and by the angle ϕ between positive x-axis and this normal line, see fig. 1. In order to determine these two parameters, the mean squared error MSE considering the perpendicular distances of N measurement points from the fitted line needs to be minimized. For this purpose, each perpendicular distance ρ_i of point i is calculated either from polar or with $x_i = r_i \cos\theta_i$ and $y_i = r_i \sin\theta_i$ alternatively in cartesian coordinates as:

$$\rho_i = d_i - d = r_i \cos(\theta_i - \phi) - d = x_i \cos\phi + y_i \sin\phi - d \tag{1}$$

Then, MSE is defined as follows dependent on ϕ and d:

$$MSE(\phi, d) = \sum_{i=1}^{N} (s_i \rho_i)^2 \tag{2}$$

In (2) optional scaling values s_i are included in order to consider an individual reliability of each measurement point. By calculating the derivatives of (2) with respect to ϕ and d and setting both to zero, the optimum values of these parameters can be analytically derived assuming all s_i to be constant, i.e. independent of ϕ and d. The solution has been published elsewhere, compare [29], yielding for ϕ and d:

$$\phi = \frac{1}{2} \cdot \operatorname{atan2}\left(-2\sigma_{xy}, \sigma_y^2 - \sigma_x^2\right) \tag{3}$$

$$d = \bar{x} \cos\phi + \bar{y} \sin\phi \tag{4}$$

The function atan2() means the four quadrant arc tangent, which calculates ϕ always in the correct range. If d becomes negative, its modulus must be taken and the corresponding ϕ has to be altered by plus or minus π. In these equations, $\bar{x}$ and $\bar{y}$ denote the mean values of all N measurements x_i and y_i, while σ_x^2, σ_y^2 and σ_{xy} denote the variances and the covariance:

$$\sigma_x^2 = \frac{1}{N} \sum_{i=1}^{N} w_i \, (x_i - \bar{x})^2 \tag{5}$$

$$\sigma_y^2 = \frac{1}{N} \sum_{i=1}^{N} w_i \, (y_i - \bar{y})^2 \tag{6}$$

$$\sigma_{xy} = \frac{1}{N} \sum_{i=1}^{N} w_i \, (x_i - \bar{x}) \, (y_i - \bar{y}) \tag{7}$$

$$\bar{x} = \frac{1}{N} \sum_{i=1}^{N} w_i x_i \tag{8}$$

$$\bar{y} = \frac{1}{N} \sum_{i=1}^{N} w_i y_i \tag{9}$$

In (5) - (9), normalized weighting factors w_i are used with $\frac{1}{N} \sum_{i=1}^{N} w_i = 1$ and $0 \leq w_i \leq 1$, calculated dependent on the chosen scaling values s_i:

$$w_i = \frac{s_i^2}{\frac{1}{N} \sum_{i=1}^{N} s_i^2} \tag{10}$$

For convenience, in the attachment a straightforward derivation of d and ϕ according to (3) and (4) is sketched.

Preprints (www.preprints.org) | NOT PEER-REVIEWED | Posted: 13 March 2018 doi:10.20944/preprints201803.0093.v1

Peer-reviewed version available at Sensors 2018, 18, 1236; doi:10.3390/s18041236

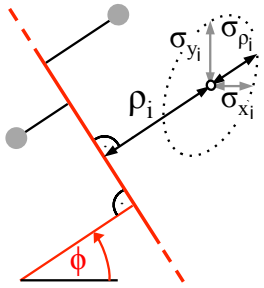

Figure 2. Optimum setting of weighting parameter for each data point

As pointed out in [32], for accurate line matching the scaling values s_i must not be assumed to be constant since in general they depend on ϕ. This can be understood from fig. 2, which shows for one measurement point i the error ellipse spanned by the standard deviations $\sigma_{x,i}$ and $\sigma_{y,i}$, while the rotation of the ellipse is caused by the covariance $\sigma_{xy,i}$.

Apparently, as a measure of confidence only the deviation $\sigma_{\rho,i}$ perpendicular to the line is relevant, while the variance of any data point in parallel to the fitted line does not influence its reliability. Thus, the angle ϕ given in (3) will only be exact, if the error ellipse equals a circle, which means that all measurements exhibit the same standard deviations in $x-$ as in $y-$direction and no covariance exist. Generally, in order to determine optimum line parameters with arbitrary variances and covariance of each measurement i, in equation (2) the inverse of $\sigma_{\rho,i}$ dependent on ϕ has to be used as scaling factor s_i, yielding:

$$MSE(\phi) = \sum_{i=1}^{N} \frac{\rho_i^2(\phi)}{\sigma_{\rho,i}^2(\phi)} \tag{11}$$

In this formula, which can only be solved numerically, the variance $\sigma_{\rho,i}^2$ needs to be calculated dependent on the covariance matrix of each measurement point i. In case of line fitting from range-bearing scans, the covariance matrix $\underline{R}_{r\theta,i}$ can be modeled as a diagonal matrix since both parameters r_i and θ_i are measured independently and thus their covariance $\sigma_{r\theta,i}$ equals zero:

$$\underline{R}_{r\theta,i} = \begin{pmatrix} \sigma_{r,i}^2 & 0 \\ 0 & \sigma_{\theta,i}^2 \end{pmatrix} \tag{12}$$

Typically, this matrix may also be considered as constant, thus independent of index i, assuming that all measured radii and angles are affected by the same noise, i.e. $\underline{R}_{r\theta,i} \approx \underline{R}_{r\theta}$.

With known variances $\sigma_{r,i}^2$ and $\sigma_{\theta,i}^2$ and for a certain ϕ, now $\sigma_{\rho,i}^2$ is determined by evaluating the relation between ρ_i and the distances d_i of each data point with $1 \leq i \leq N$. According to (1) and with the distance d written as mean of all d_i it follows:

$$\rho_i = d_i - \frac{1}{N}\sum_{j=1}^{N} d_j = \left(\frac{N-1}{N}\right) d_i - \frac{1}{N}\sum_{\substack{j=1 \\ (j\neq i)}}^{N} d_j \tag{13}$$

Since noise induced variations of all distances d_i are uncorrelated to each other, now the variance $\sigma_{\rho,i}^2$ is calculated by means of summing over all variances $\sigma_{d,i}^2$:

$$\sigma_{\rho,i}^2 = \left(\frac{N-1}{N}\right)^2 \sigma_{d,i}^2 + \frac{1}{N^2}\sum_{\substack{j=1 \\ (j\neq i)}}^{N} \sigma_{d,j}^2 \tag{14}$$

Peer-reviewed version available at Sensors 2018, 18, 1236; doi:10.3390/s18041236

In order to derive $\sigma_{d,i}^2$, changes of d_i with respect to small deviations of r_i and θ_i from their expected values $\bar{r}_i$ and $\bar{\theta}_i$ are considered with $d_i = \bar{d}_i + \Delta d_i$, $r_i = \bar{r}_i + \Delta r_i$ and with $\theta_i = \bar{\theta}_i + \Delta\theta_i$:

$$\Delta d_i = \Delta d_i^r + \Delta d_i^\theta \tag{15}$$

The terms on the right side of (15) can be determined independently of each other, since Δr_i and $\Delta\theta_i$ are assumed to be uncorrelated. With $d_i = r_i \cdot \cos(\theta_i - \phi)$ it follows

$$\Delta d_i^r = \Delta r_i \cdot \cos(\bar{\theta}_i - \phi) \tag{16}$$

and

$$\Delta d_i^\theta = \bar{r}_i \left[\cos(\bar{\theta}_i - \phi + \Delta\theta_i) - \cos(\bar{\theta}_i - \phi)\right] \approx -\bar{r}_i \left[\frac{\Delta\theta_i^2}{2}\cos(\bar{\theta}_i - \phi) + \Delta\theta_i \sin(\bar{\theta}_i - \phi)\right] \tag{17}$$

In the last line the addition theorem was applied for $\cos(\bar{\theta}_i - \phi + \Delta\theta_i)$, and for small variations the approximations $\cos(\Delta\theta_i) \approx 1 - \frac{\Delta\theta_i^2}{2}$ and $\sin(\Delta\theta_i) \approx \Delta\theta_i$ are valid.

The random variables Δr_i and $\Delta\theta_i$ are assumed to be normally distributed with variances $\sigma_{r,i}^2$ and $\sigma_{\theta,i}^2$. Thus, the random variable $\Delta\theta_i^2$ exhibits a χ^2-distribution with variance $2(\sigma_{\theta,i}^2)^2$, see [41], and the variance of d_i is calculated from (15), (16) and (17) as weighted sum with $\bar{r}_i$ and $\bar{\theta}_i$ approximately replaced by r_i and θ_i, respectively:

$$\sigma_{d,i}^2 = \left(\sigma_{r,i}^2 + \frac{(\sigma_{\theta,i}^2)^2}{2}\right)\cos^2(\theta_i - \phi) + \sigma_{\theta,i}^2 \sin^2(\theta_i - \phi) \tag{18}$$

When applying this algorithm, a one-dimensional minimum search of MSE according to (11) needs to be executed, yielding the optimum ϕ of the straight line. For this purpose, $\sigma_{\rho,i}^2$ is inserted from (14) considering (18), and ρ_i is determined according to (1) by calculating d from (4), (8), (9) and (10) with $s_i = 1/\sigma_{\rho,i}$.

Obviously, numerical line fitting can also be accomplished if measurements are available in cartesian coordinates x_i and y_i. In this case, the covariance matrix $\underline{R}_{xy,i}$ of each measurement point must be known, defined as:

$$\underline{R}_{xy,i} = \begin{pmatrix} \sigma_{x,i}^2 & \sigma_{xy,i} \\ \sigma_{xy,i} & \sigma_{y,i}^2 \end{pmatrix} \tag{19}$$

Furthermore, the partial derivatives of d_i according to (1) with respect to x_i and y_i need to be calculated:

$$\underline{J}_{d,i} = \begin{pmatrix} \frac{\partial d_i}{\partial x_i} & \frac{\partial d_i}{\partial y_i} \end{pmatrix} = \begin{pmatrix} \cos\phi & \sin\phi \end{pmatrix} \tag{20}$$

Then, $\sigma_{d,i}^2$ follows dependent on $\underline{R}_{xy,i}$ and $\underline{J}_{d,i}$:

$$\sigma_{d,i}^2 = \underline{J}_{d,i} \cdot \underline{R}_{xy,i} \cdot (\underline{J}_{d,i})^T = \sigma_{x,i}^2 \cos^2\phi + \sigma_{xy,i} \sin\phi\cos\phi + \sigma_{y,i}^2 \sin^2\phi \tag{21}$$

If raw data stems from a range-bearing scan, $\underline{R}_{xy,i}$ can be calculated from $\underline{R}_{r\theta,i}$ by exploiting the known dependencies between the polar- and cartesian plane. For this purpose the Jacobian matrix $\underline{J}_{xy,i}$ is determined:

$$\underline{J}_{xy,i} = \begin{pmatrix} \frac{\partial x_i}{\partial r_i} & \frac{\partial x_i}{\partial \theta_i} \\ \frac{\partial y_i}{\partial r_i} & \frac{\partial y_i}{\partial \theta_i} \end{pmatrix} = \begin{pmatrix} \cos\theta_i & -r_i \sin\theta_i \\ \sin\theta_i & r_i \cos\theta_i \end{pmatrix} \tag{22}$$

Peer-reviewed version available at Sensors 2018, 18, 1236; doi:10.3390/s18041236

Then, the covariance matrix $\underline{R}_{xy,i}$ will depends on $\underline{R}_{r\theta,i}$, if small deviations from the mean value of the random variables r_i and θ_i and a linear model are assumed:

$$\underline{R}_{xy,i} = \underline{J}_{xy,i} \cdot \underline{R}_{r\theta,i} \cdot (\underline{J}_{xy,i})^T \tag{23}$$

According to (23) generally a strong covariance $\sigma_{xy,i}$ in $\underline{R}_{xy,i}$ must be considered, if measurements are taken by range-bearing sensors.

By means of applying (21) to (23) instead of (18) for searching the minimum of MSE dependent on ϕ, the second order effect regarding $\Delta\theta_i$ is neglected. This yields almost the same formula as given in [32], though the derivation differs and in [32] additionally the variance of d is ignored assuming $\sigma^2_{\rho,i} = \sigma^2_{d,i}$, which according to (14) is only asymptotically correct for large N.

Finally, it should be noted that the numerical determination of ϕ according to (11) means clearly more complexity compared to the straightforward solution according to equation (3). Later, in chapter 5 it will be analyzed under which conditions this additional computational effort actually is required.

3. Analytic error models of straight lines

In literature several methods are described to estimate errors of ϕ and d and their mutual dependency. Thus, the covariance matrix $R_{d\phi}$ must be known, defined as:

$$\underline{R}_{d\phi} = \begin{pmatrix} \sigma_d^2 & \sigma_{d\phi} \\ \sigma_{d\phi} & \sigma_\phi^2 \end{pmatrix} \tag{24}$$

For this purpose, a general method in nonlinear parameter estimation is the calculation of the inverse Hessian matrix at the minimum of MSE. Details can be found in [27] and [32], while in [42] it is shown that this procedure may exhibit numerical instability. In section 5, results using this method are compared with other approaches.

Alternatively, in [29] and [43] an analytic error model is proposed based on fault analysis of the line parameters. In this approach, the effect of variations of each single measurement point defined by $\underline{R}_{xy,i}$ with respect to the covariance matrix of the line parameters $\underline{R}_{d\phi}$ is considered, based on (3) and (4). Thereto, the Jacobian matrix $\underline{J}_{d\phi,i}$ with respect to x_i and y_i is determined, defined as:

$$\underline{J}_{d\phi,i} = \begin{pmatrix} \frac{\partial d}{\partial x_i} & \frac{\partial d}{\partial y_i} \\ \frac{\partial \phi}{\partial x_i} & \frac{\partial \phi}{\partial y_i} \end{pmatrix} \tag{25}$$

With this matrix the contribution of a single data point i to the covariance matrix between d and ϕ can be written as:

$$\underline{R}_{d\phi,i} = \underline{J}_{d\phi,i} \cdot \underline{R}_{xy,i} \cdot \underline{J}^T_{d\phi,i} \tag{26}$$

For determining the partial derivatives of d in (25), equation (4) is differentiated after expanding it by (8) and (9), yielding:

$$\frac{\partial d}{\partial x_i} = w_i \frac{\cos\phi}{N} + (\bar{y}\cos\phi - \bar{x}\sin\phi)\frac{\partial \phi}{\partial x_i} \tag{27}$$

$$\frac{\partial d}{\partial y_i} = w_i \frac{\sin\phi}{N} + (\bar{y}\cos\phi - \bar{x}\sin\phi)\frac{\partial \phi}{\partial y_i} \tag{28}$$

Differentiating ϕ according to (3) with respect to x_i gives the following expression with $u = -2\sigma_{xy}$ and $v = \sigma_y^2 - \sigma_x^2$:

$$\frac{\partial \phi}{\partial x_i} = \frac{1}{2(u^2+v^2)}\left(\frac{\partial u}{\partial x_i}v - \frac{\partial v}{\partial x_i}u\right) \tag{29}$$

The partial derivation of u in (29) is calculated after expanding it with (7) and (8) as:

$$\frac{\partial u}{\partial x_i} = -\frac{2}{N} \cdot \frac{\partial}{\partial x_i} \left(\sum_{i=1}^{N} w_i x_i y_i - \bar{y} \sum_{i=1}^{N} w_i x_i \right) = -\frac{2w_i}{N} \left(y_i - \bar{y} \right) \tag{30}$$

while partial derivation of v with (5), (6) and (8) yields:

$$\frac{\partial v}{\partial x_i} = -\frac{1}{N} \cdot \frac{\partial}{\partial x_i} \left(\sum_{i=1}^{N} w_i x_i^2 - \frac{1}{N} \left(\sum_{i=1}^{N} w_i x_i \right)^2 \right) = -\frac{2w_i}{N} \left(x_i - \bar{x} \right) \tag{31}$$

Finally, after substituting all terms with u and v in (29) it follows:

$$\frac{\partial \phi}{\partial x_i} = w_i \frac{\left(\sigma_x^2 - \sigma_y^2 \right) \left(y_i - \bar{y} \right) - 2\sigma_{xy} \left(x_i - \bar{x} \right)}{N \left(\left(\sigma_x^2 - \sigma_y^2 \right)^2 + 4\sigma_{xy}^2 \right)} \tag{32}$$

Correspondingly, for the partial derivative of ϕ with respect to y_i the following result is obtained:

$$\frac{\partial \phi}{\partial y_i} = w_i \frac{\left(\sigma_x^2 - \sigma_y^2 \right) \left(x_i - \bar{x} \right) + 2\sigma_{xy} \left(y_i - \bar{y} \right)}{N \left(\left(\sigma_x^2 - \sigma_y^2 \right)^2 + 4\sigma_{xy}^2 \right)} \tag{33}$$

Now, after inserting (27), (28), (32) and (33) into (25) the covariance matrix of d and ϕ (24) is calculated by summing over all N data points since the noise contributions of the single measurements can be assumed to be stochastically independent of each other:

$$\underline{R}_{d\phi} = \sum_{i=1}^{N} \underline{R}_{d\phi,i} = \sum_{i=1}^{N} \underline{J}_{d\phi,i} \cdot \underline{R}_{xy,i} \cdot \underline{J}_{d\phi,i}^T \tag{34}$$

Equation (34) enables an exact calculation of the variances σ_d^2, σ_ϕ^2 and of the covariance $\sigma_{d\phi}$ as long as the deviations of the measurements stay within the range of a linear approach, and as long as equations (3) and (4) are valid. In contrast to the method proposed in [32] no second derivatives and no inversion of the Hessian matrix are needed and thus more stable results can be expected.

However, both algorithms need some computational effort especially for a large number of measurement points. Moreover, they do not allow to understand the effect of changing parameters on $R_{d\phi}$, and these models can only be applied, if for each data point the covariance matrix $\underline{R}_{xy,i}$ is available. Unfortunately, for lines extracted from images this information is unknown, and also in case of using range-bearing sensors just a worst case estimate of σ_r is given in data sheet while σ_θ is ignored.

4. Closed-form error model of a straight line

In this section a simplified error model in closed form is deduced, which enables a fast, clear and yet for most applications sufficiently accurate calculation of the covariance matrix $\underline{R}_{d\phi}$ in any case when line parameters d and ϕ have been determined from a number of discrete data points.

Thereto, first the expected values of the line parameters d and ϕ, denoted as $\bar{d}$ and $\bar{\phi}$, are assumed to be known according to the methods proposed in section 2 with $\bar{d} \approx d$ and $\bar{\phi} \approx \phi$. Besides, for modeling the small deviation of d and ϕ, the random variables Δd and $\Delta\phi$ are introduced. Thus, with $d = \bar{d} + \Delta d$ and $\phi = \bar{\phi} + \Delta\phi$ it follows for the variances and the covariance:

$$\sigma_d^2 = \sigma_{\Delta d}^2 \qquad \sigma_\phi^2 = \sigma_{\Delta\phi}^2 \qquad \sigma_{d\phi} = \sigma_{\Delta d \Delta\phi} \tag{35}$$

Preprints (www.preprints.org) | NOT PEER-REVIEWED | Posted: 13 March 2018 doi:10.20944/preprints201803.0093.v1

Peer-reviewed version available at Sensors 2018, 18, 1236; doi:10.3390/s18041236

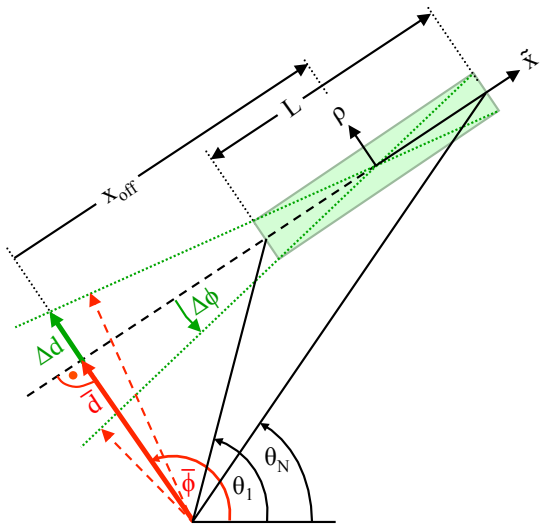

Figure 3. Dependency between Δd, $\Delta\phi$ and geometric parameters

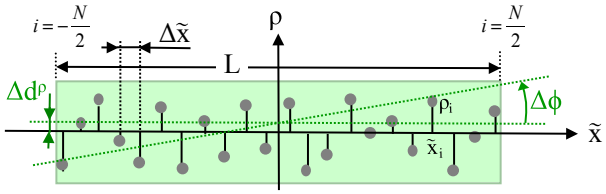

Figure 4. Details of fig. 3 with the deviation of data points along the axis $\tilde{x}$

Next, Δd and $\Delta\phi$ shall be determined dependent on a random variation of any of the N measured data points. For this purpose, fig. 3 is considered, which shows the expected line parameters and the random variables Δd and $\Delta\phi$.

In order to derive expressions for Δd and $\Delta\phi$ depending on the random variables ρ_i, fig. 4 shows an enlargement of the rectangular box depicted in fig. 3 along the direction of the line $\tilde{x}$.

First, the effect of variations of any ρ_i on $\Delta\phi$ is considered. Since $\Delta\phi$ is very small, this angle may be replaced by its tangent, which defines the slope Δm of the line with respect to the direction $\tilde{x}$. Here, only ρ_i is considered as a random variable but not $\tilde{x}_i$. Thus, the standard formula for the slope of a regression line can be applied, which will minimize the mean squared distance in the direction of ρ, if all $\tilde{x}_i$ are assumed to be exactly known:

$$\Delta\phi \approx \tan(\Delta\phi) = \Delta m = \frac{\sigma_{\rho\tilde{x}}}{\sigma_{\tilde{x}}^2} = \frac{\sum\limits_i \rho_i \cdot \tilde{x}_i}{\sum\limits_i \tilde{x}_i^2} \tag{36}$$

Now, in order to calculate the variance of $\Delta\phi$, a linear relation between $\Delta\phi$ and each ρ_i is required, which is provided by the first derivation of (36) with respect to ρ_i:

$$\frac{\partial\Delta\phi}{\partial\rho_i} = \frac{\tilde{x}_i}{\sum\limits_i \tilde{x}_i^2} \tag{37}$$

Then, the variance of $\Delta\phi$ dependent on the variance of ρ_i can be specified. From (37) it follows:

Preprints (www.preprints.org) | NOT PEER-REVIEWED | Posted: 13 March 2018 doi:10.20944/preprints201803.0093.v1

Peer-reviewed version available at Sensors 2018, 18, 1236; doi:10.3390/s18041236

$$\sigma_{\Delta\phi,i}^2 = \sigma_{\rho,i}^2 \cdot \left(\frac{\partial\Delta\phi}{\partial\rho_i}\right)^2 = \sigma_{\rho,i}^2 \cdot \frac{\tilde{x}_i^2}{\left(\sum_i \tilde{x}_i^2\right)^2} \tag{38}$$

If $\sigma_{\rho,i}^2$ is assumed to be approximately independent of i, it may be replaced by σ_ρ^2 and can be estimated from (2) with ρ_i taken from (1) and setting all s_i to $1/N$:

$$\sigma_{\rho,i}^2 \approx \sigma_\rho^2 = \frac{1}{N}\sum_{i=1}^{N} \rho_i(\phi, d)^2 \tag{39}$$

It should be noted, that for a bias-free estimation of σ_ρ^2 with (39), the exact line parameters ϕ and d must be used in (1), which obviously are not available. If instead estimated line parameters according to chapter 2 are taken, e. g. by applying (3) and (4), calculated from the same data as used in (39), an underestimation of σ_ρ^2 especially for small N can be expected, since ϕ and d are determined by minimizing the variance of ρ of these N data points. This is referred to later.

Next, from (38) the variance of $\Delta\phi$ results as sum over all N data points, since all ρ_i are independent of each other:

$$\sigma_{\Delta\phi}^2 = \sum_i \sigma_{\Delta\phi,i}^2 \approx \sigma_\rho^2 \cdot \frac{\sum_i \tilde{x}_i^2}{\left(\sum_i \tilde{x}_i^2\right)^2} = \sigma_\rho^2 \cdot \frac{1}{\sum_i \tilde{x}_i^2} \tag{40}$$

Equation (40) with (35) and (39) enables an exact calculation of σ_ϕ^2 dependent on the N data points of the line.

However, from (40) a straightforward expression can be derived, which is sufficiently accurate in most cases and enables a clear understanding of the influencing parameters on σ_ϕ^2, compare section 5. For this purpose, according to fig. 3 the length L of a line segment is determined from the perpendicular distance d and from the angles θ_1 and θ_N of the 1st and Nth data point, respectively:

$$L = d \cdot |\tan(\phi - \theta_N) - \tan(\phi - \theta_1)| \tag{41}$$

Furthermore, a constant spacing $\Delta\tilde{x}$ between adjacent data points is assumed:

$$\Delta\tilde{x} \approx \frac{L}{N-1}. \tag{42}$$

Applying this approximation, the sum over all squared $\tilde{x}_i$ can be rewritten, yielding for even N as depicted in fig. 4:

$$\sum_i \tilde{x}_i^2 \approx 2 \cdot \sum_{i=1}^{N/2} \left[\frac{\Delta\tilde{x}}{2}(2i-1)\right]^2 = \Delta\tilde{x}^2 \cdot \sum_{i=1}^{N/2} \frac{(2i-1)^2}{2} \tag{43}$$

The last sum can be transformed into closed form as:

$$\sum_{i=1}^{N/2} \frac{(2i-1)^2}{2} = \frac{\frac{N}{2}\left(4\left(\frac{N}{2}\right)^2 - 1\right)}{6} = \frac{N(N^2-1)}{12} \tag{44}$$

With N odd, the sum must be taken twice from 1 to $\frac{N-1}{2}$ since in this case the central measurement point has no effect on $\sigma_{\Delta\phi,i}^2$, yielding:

$$\sum_i \tilde{x}_i^2 \approx 2 \cdot \sum_{i=1}^{\frac{(N-1)}{2}} [\Delta\tilde{x} \cdot i]^2 = \Delta\tilde{x}^2 \cdot \sum_{i=1}^{\frac{(N-1)}{2}} 2 \cdot i^2 \tag{45}$$

Preprints (www.preprints.org) | NOT PEER-REVIEWED | Posted: 13 March 2018 doi:10.20944/preprints201803.0093.v1

Peer-reviewed version available at Sensors 2018, 18, 1236; doi:10.3390/s18041236

Again, the last sum can be written in closed form, which gives the same result as in (44):

$$\sum_{i=1}^{\frac{(N-1)}{2}} 2 \cdot i^2 = \frac{\frac{N-1}{2}\left(\frac{N-1}{2}+1\right)\left(2 \cdot \frac{N-1}{2}+1\right)}{3} = \frac{N(N^2-1)}{12} \tag{46}$$

Finally, by substituting (43) with (44), or (45) with (46) into (40) and regarding (35) as well as (42), a simple analytic formula for calculating the variance of ϕ is obtained, just depending on L, N and the variance of ρ:

$$\sigma_\phi^2 \approx \sigma_\rho^2 \cdot \frac{12}{L^2 \cdot N} \cdot \frac{N-1}{N+1} \overset{N \gg 1}{\approx} \sigma_\rho^2 \cdot \frac{12}{L^2 \cdot N} \tag{47}$$

The last simplification in (47) overestimates σ_ϕ^2 a little bit for small N. Interestingly, this error compensates quite well for a certain underestimation of σ_ρ^2 according to (39), assuming that the line parameters ϕ and d are determined from the same data as σ_ρ^2, see chapter 5.

Next, in order to deduce the variance σ_d^2, again fig. 3 is considered. Apparently, a first part of the random variable Δd is strongly correlated to $\Delta\phi$ since any mismatch in ϕ is transformed into a deviation Δd by means of the geometric offset x_{off} with:

$$\Delta d^\phi = -x_{off} \cdot \Delta\phi \tag{48}$$

Actually, with a positive value for x_{off} as depicted in fig. 3 the correlation between Δd and $\Delta\phi$ becomes negative, since positive values of $\Delta\phi$ correspond to negative values of Δd. According to fig. 3, x_{off} is determined from ϕ and d as well as from θ_1 and θ_N:

$$x_{off} = \frac{d}{2} \cdot [\tan(\phi - \theta_N) + \tan(\phi - \theta_1)] \tag{49}$$

Alternatively, x_{off} can be taken as mean value from all N data points of the line segment:

$$x_{off} = \frac{d}{N} \cdot \sum_{i=1}^{N} \tan(\phi - \theta_i) \tag{50}$$

Nevertheless, it should be noted that Δd is not completely correlated with $\Delta\phi$, since also in the case $x_{off} = 0$ the error Δd will not be zero.

Indeed, as a second effect each single ρ_i has a direct linear impact on the variable Δd. For this purpose, in fig. 4 the random variable Δd^ρ is depicted, which describes a parallel shift of the regression line due to variation in ρ_i, calculated as mean value over all ρ_i:

$$\Delta d^\rho = \frac{1}{N} \cdot \sum_i \rho_i \tag{51}$$

Combining both effects, variations in d can be described as the sum of two uncorrelated terms, Δd^ϕ and Δd^ρ:

$$\Delta d = \Delta d^\phi + \Delta d^\rho = -x_{off} \cdot \Delta\phi + \frac{1}{N} \cdot \sum_i \rho_i \tag{52}$$

This missing correlation between $\Delta\phi$ and the sum over all ρ_i is also intuitively accessible: If the latter takes a positive number it will not be possible to deduce the sign or the modulus of $\Delta\phi$. From (52) and with $E(\Delta d^\phi \cdot \Delta d^\rho) = 0$, $E(\Delta d^\phi) = 0$ and $E(\Delta d^\rho) = 0$ the variance σ_d^2 can be calculated as

$$\sigma_d^2 = E([\Delta d]^2) = E([\Delta d^\phi]^2) + E([\Delta d^\rho]^2) = x_{off}^2 \cdot E([\Delta\phi]^2) + \frac{1}{N^2} \cdot E\left(\left[\sum_i \rho_i\right]^2\right) \tag{53}$$

Preprints (www.preprints.org) | NOT PEER-REVIEWED | Posted: 13 March 2018 doi:10.20944/preprints201803.0093.v1

Peer-reviewed version available at Sensors 2018, 18, 1236; doi:10.3390/s18041236

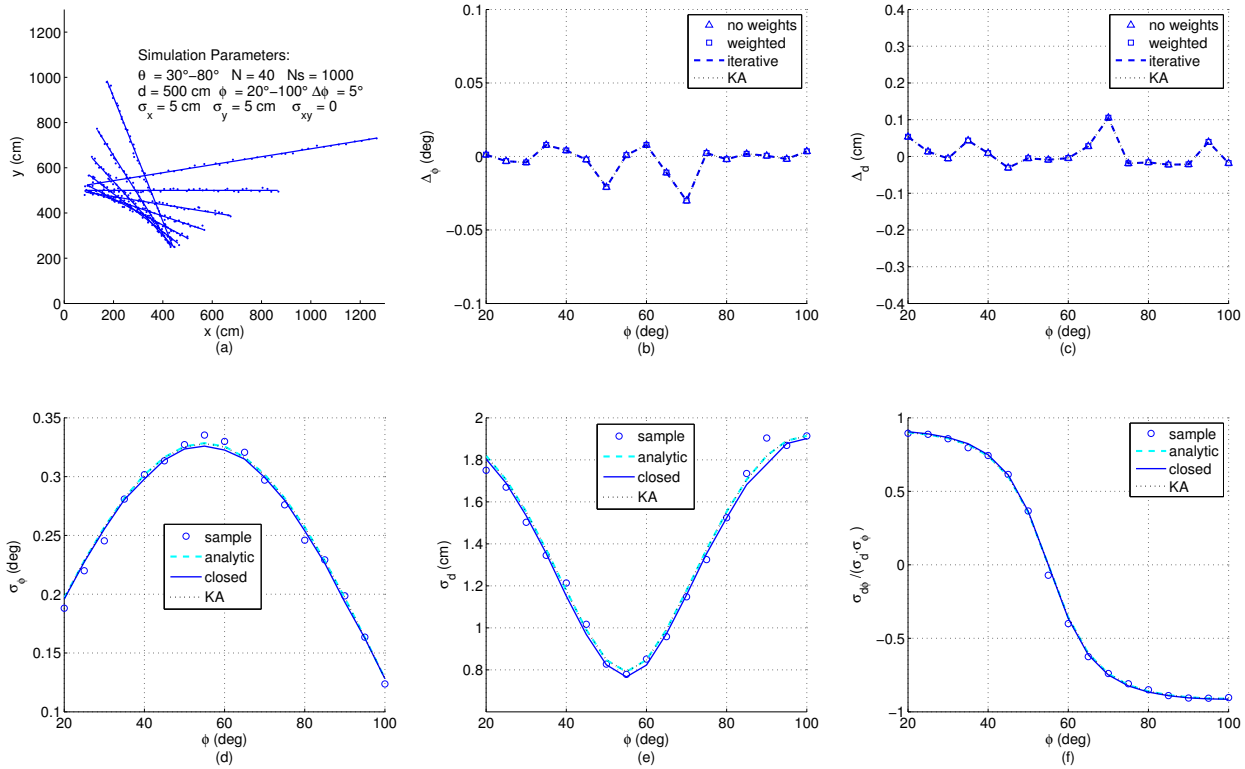

Figure 5. Simulation Results for equidistant measurement points superimposing normal distributed and uncorrelated noise in x- and y-direction

$$\approx x_{off}^2 \cdot \sigma_\phi^2 + \frac{1}{N} \cdot \sigma_\rho^2 \tag{54}$$

In the last step from (53) to (54) again the independence of the single measurements from each other is used, thus the variance of the sum of the N data points approximates N-times the variance σ_ρ^2. Finally, the covariance between ϕ and d needs to be determined. Based on the definition it follows with $\sigma_{d\phi} = \sigma_{\Delta d \Delta \phi}$

$$\sigma_{d\phi} = E(\Delta d \cdot \Delta\phi) = E(\Delta d^{\phi} \cdot \Delta\phi) + E(\Delta d^{\rho} \cdot \Delta\phi) = -x_{off} \cdot E([\Delta\phi]^2) = -x_{off} \cdot \sigma_\phi^2 \tag{55}$$

By means of (47), (54) and (55), now the complete error model in closed form is known, represented by the covariance matrix $\underline{R}_{d\phi}$ given as:

$$\underline{R}_{d\phi} \approx \sigma_\rho^2 \cdot \begin{pmatrix} \frac{12 \cdot x_{off}^2}{L^2 \cdot N} + \frac{1}{N} & \frac{-12 \cdot x_{off}}{L^2 \cdot N} \\ \frac{-12 \cdot x_{off}}{L^2 \cdot N} & \frac{12}{L^2 \cdot N} \end{pmatrix} \tag{56}$$

Applying this error model is easy since no knowledge of the variances and covariance for each single measurement is needed, which in practice is difficult to acquire. Instead, just the number N of preferably equally spaced points used for line fitting, the length L of the line segment, its offset x_{off} and the variance σ_ρ^2 according to (41), (49) and (39) must be inserted.

5. Simulation results

The scope of this section is to compare the presented algorithms for linear regression and error modeling based on statistical evaluation of the results. Segmentation of raw data is not considered; if necessary this must be performed beforehand by means of well-known methods

Peer-reviewed version available at Sensors 2018, 18, 1236; doi:10.3390/s18041236

like Hough-Transformation or RANSAC, compare section 1. Thus, for studying the performance reliably and repeatably, a large number of computer simulations was performed, applying a systematic variation of parameters within a wide range, which would not be feasible if real measurement are used.

For this purpose, straight lines with a certain perpendicular distance d from origin and within a varying range of normal angles ϕ have been specified. Each of these lines is numerical described by a number of N points either given in cartesian (x_i, y_i) or in polar $(r_i\ \theta_i)$ coordinates. In order to simulate the outcome of a real range-bearing sensor as close as possible, the angular coordinate was varied between θ_1 and θ_N. To each measurement a certain amount of normally distributed noise with σ_x, σ_y and σ_{xy} or alternatively with σ_r and σ_θ was added. Further, for each ϕ a number of $N_s = 1000$ sets of samples was generated, in order to allow statistical evaluation of the results. A first simulation was performed with $N = 40$ equally spaced points affected each by uncorrelated noise in $x-$ and $y-$direction with standard deviations $\sigma_x = \sigma_y = 5\,cm$. This is a typical situation when a line is calculated from binary pixels, and in subfigure (a) of fig. 5 a bundle of the simulated line segments is shown. The deviations Δ_ϕ and Δ_d taken as mean value over all N_s samples of the estimated ϕ and d from their true values, respectively, are depicted in subfigures (b) and (c) comparing four algorithms as presented in section 2: The triangles mark the outcome of equations (3) and (4) with all weights set to one, whereas the squares are calculated according to the same analytic formulas but using individual weighting factors applying (10) with $s_i = 1/\sigma_{\rho,i}$. The perpendicular deviations $\sigma_{\rho,i}$ are determined according to (14) and (21) with ϕ taken from (3) without weights. Obviously, in this example all triangles coincide with the squares since each measurement i is affected by the same noise and thus for any ϕ all weighting factors are always identical. The dashed lines in (b) and (c) show the results when applying the iterative method according to (11) with the minimum of MSE found numerically. For this purpose, $\sigma^2_{\rho,i}$ is inserted from (14) considering (21), ρ_i is taken from (1) and d is calculated from (4), (8), (9) and (10) with $s_i = 1/\sigma_{\rho,i}$. The dotted lines (KA) depict the deviations of d and ϕ obtained according to Krystek and Anton in [32]. Both numerical algorithm yield the same results, which is not surprising, since the variances $\sigma^2_{\rho,i}$ used as weighting factors are all identical. Further, here the analytical algorithms provide exactly the same performance as the numerical ones, since for $\sigma_x = \sigma_y$ the weighting factors show no dependency on ϕ and for that case the analytical formulas are optimal.

The lower subfigures depict the parameters of the covariance matrix $\underline{R}_{d\phi}$ again as a function of ϕ comparing different methods. Here, the circles represent numerical results obtained from the definitions of variance and covariance by summing over all N_s passes with $1 \leq k \leq N_s$, yielding d_k and ϕ_k, respectively:

$$\sigma_d^2 = \frac{1}{N_s} \sum_{k=1}^{N_s} (d_k - d)^2 \tag{57}$$

$$\sigma_\phi^2 = \frac{1}{N_s} \sum_{k=1}^{N_s} (\phi_k - \phi)^2 \tag{58}$$

$$\sigma_{d\phi} = \frac{1}{N_s} \sum_{k=1}^{N_s} (d_k - d)\,(\phi_k - \phi) \tag{59}$$

Since these numerical results serve just as reference for judging the accuracy of the error models, in the formulas above the true values for d and ϕ have been used. The required line parameters d_k and ϕ_k in (57) - (59) can be estimated with any of the described four methods, since minor differences in d_k and ϕ_k have almost no effect on the resulting variances and the covariance. The dashed lines in subfigures (d) - (f) show the results of the analytic error model as described in section 3, and the dotted lines represent the outcomes of the algorithm from Krystek and Anton [32], while the continuous line corresponds to the model in closed-form according to (56) in section 4 with L and x_{off} taken from (41) and (49), respectively. Interestingly, although the theoretical derivations differ

Preprints (www.preprints.org) | NOT PEER-REVIEWED | Posted: 13 March 2018 doi:10.20944/preprints201803.0093.v1

Peer-reviewed version available at Sensors 2018, 18, 1236; doi:10.3390/s18041236

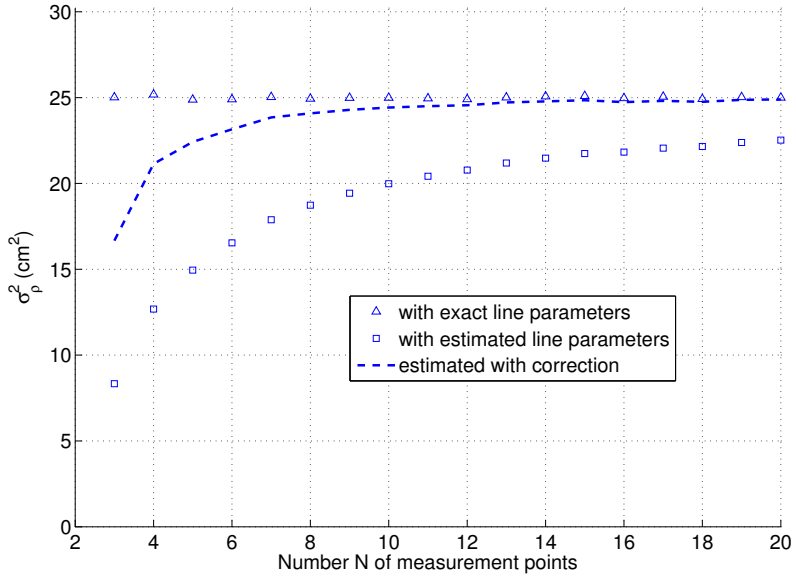

Figure 6. Variance of ρ dependent on the number N of measured data points, using the same simulation parameters as indicated in figure 5(a)

substantially, the results match very well, which especially proves the correctness of the simplified model in closed-form. Since this model explicitly considers the effect of the line length L and of the geometric offset x_{off}, the behavior of the curves can be clearly understood: The minimum of L will occur if ϕ equals the mean value of θ_{min} and θ_{max}, i.e. at $\phi = 55°$, and exactly at this angle the maximum standard deviation σ_ϕ occurs. Further, since L linearly depends on ϕ, a quadratic dependence of σ_ϕ on ϕ according to (47) can be observed. With respect to fig. 5(e) the minimum of σ_d also appears at $\phi = 55°$ corresponding to $x_{off} = 0$. At this angle according to (54) the standard deviation of d is given as $\sigma_d \approx \sigma_\rho / \sqrt{N} = 5/\sqrt{40} = 0.79$, while the covariance $\sigma_{\rho d}$ calculated according to (55) and with it the correlation coefficient shown in fig. 5(f) vanishes.

When comparing the results, one should be aware that in the simulations of the analytic error models the exact variances $\sigma_{x_i}^2$, $\sigma_{y_i}^2$ and σ_{xy_i} are used, thus in practice achievable accuracies will be worse. On the other hand, when applying the new error model in closed-form, the variance σ_ρ^2 is calculated as mean value of all ρ_i^2 from the actual set of N data points according to (39) and hence is always available.

Nevertheless, if in this equation the estimated line parameters ϕ and d are used, which are calculated e. g. according to (3) and (4) using the same measurements as in (39), no unbiased σ_ρ^2 can be expected. This is reasoned from the fact that for each set of N data points, the mean quadratic distance over all ρ_i^2 is minimized in order to estimate ϕ and d. Thus, the numeric value of σ_ρ^2 will always be smaller than its correct value calculated with the exact line parameters. This effect can be clearly observed from fig. 6, which shows for the same simulation parameters as depicted in fig. 5(a) the dependency of σ_ρ^2 on the number of points on the line N, averaged over N_s sets of samples: Only in case of using the exact line parameters in (39), which obviously are only available in a simulation, actually the correct $\sigma_\rho^2 = 25\,cm^2$ is obtained as shown by the triangles. If however at each run σ_ρ^2 is calculated with the estimated ϕ and d as indicated by the squares, a clear deviation especially at low N occurs. Only asymptotically for large N when ϕ converges to its exact value the correct σ_ρ^2 is reached. Fortunately, this error can be compensated quite well by means of multiplying σ_ρ^2 with a correction factor $c = \frac{N+1}{N-1}$ as shown by the dashed line in fig. 6. Due to the strongly non-linear relation between ϕ and any ρ_i, this correction works much better than simply exchanging in (39) the divisor N by $N-1$ as often used in statistics. Since c is the inverse of the term neglected in the approximation of σ_ϕ^2 in

Preprints (www.preprints.org) | NOT PEER-REVIEWED | Posted: 13 March 2018 doi:10.20944/preprints201803.0093.v1

Peer-reviewed version available at Sensors 2018, 18, 1236; doi:10.3390/s18041236

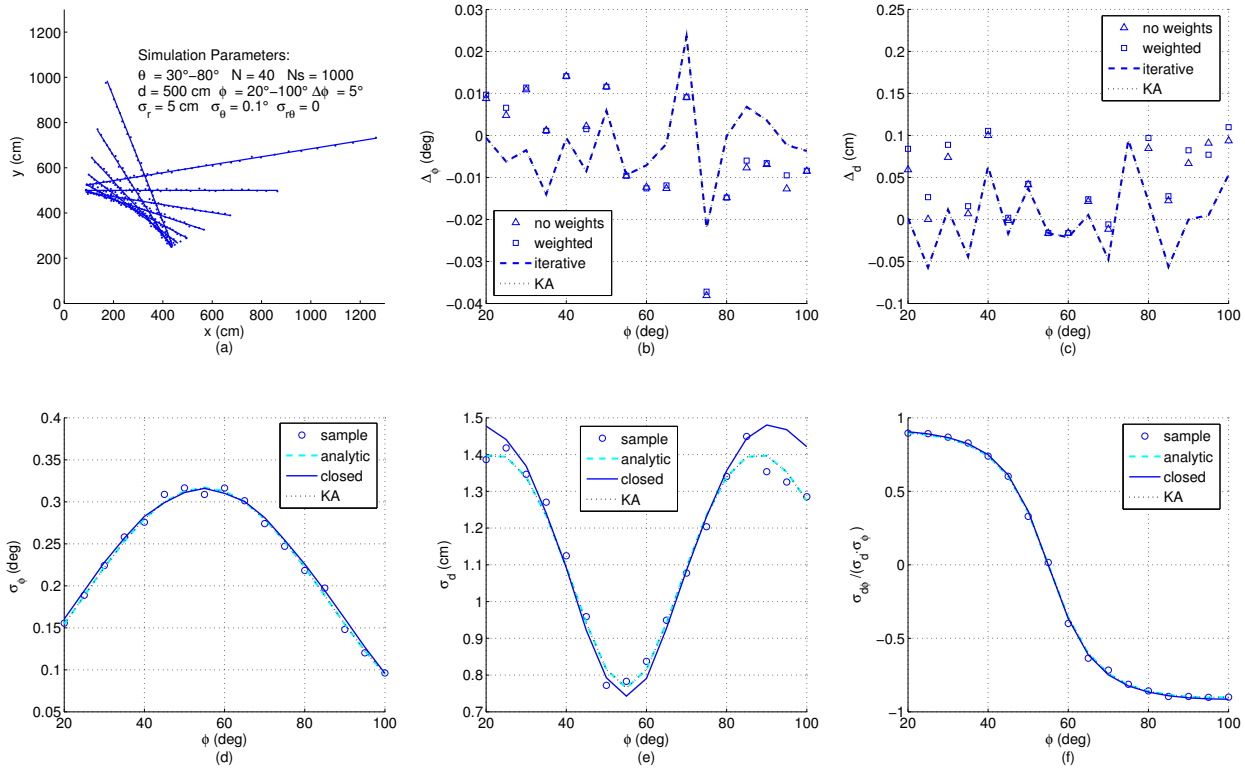

Figure 7. Results from simulated range-bearing scans superimposing low noise in r- and θ-direction

(47), the closed-form of the covariance matrix $\underline{R}_{d\phi}$ according to (56) yields almost unbiased results also for small N if σ_ρ^2 is calculated according to (39) with estimated line parameters ϕ and d. Although not shown here, the proposed bias compensation works well for a large range of measurement parameters. For a reliable determination of σ_ρ^2 from N data points of a line segment, N should be at least in the order of 10.

Figure 7 shows the results when simulating a range-bearing scan with a constant angular offset $\Delta\theta = (\theta_{max} - \theta_{min})/(N-1)$ between adjacent measurements. Each measurement is distorted by adding normally distributed noise with standard deviations $\sigma_r = 5\,cm$ and $\sigma_\theta = 0.1°$. This is a more challenging situation, since now the measurements are not equispaced, each data point exhibits individual variances $\sigma_{x,i}$, $\sigma_{y,i}$ dependent on ϕ, and moreover a covariance $\sigma_{xy,i}$ exists. As can be seen, the errors of the estimated ϕ and d as depicted in subfigure (b) and (c) exhibit the same order of magnitude as before, yet, both analytic results differ slightly from each other and are less accurate compared to the numerical solutions. Both numerical methods yield quasi identical results, since for the chosen small noise amplitudes the differences between both algorithms have no impact on the resulting accuracy.

Regarding the error models, subfigures (d) to (f) reveal, that in spite of unequal distances between the measurement points and varying $\sigma_{\rho,i}$ the results of the closed-form model match well with the analytic and numeric results. Only σ_d shows a certain deviation at steep and flat lines with ϕ below 30° or above 80°. This is related to errors in x_{off}, since in this range of ϕ the points on the lines measured with constant $\Delta\theta$ have clearly varying distances and thus (49) yields just an approximation of the effective offset of the straight line.

The next figure 8 shows the results with the models applied to short lines measured in the angular range of $30° \leq \theta \leq 40°$ with $N = 20$, while all other parameters are identical to those depicted in fig. 7(a). As can be seen from subfigures (b) and (c), now the analytical algorithms based on (3) and (4) are no longer adequate since these, independent of applying weights or not, yield much higher errors

Preprints (www.preprints.org) | NOT PEER-REVIEWED | Posted: 13 March 2018 doi:10.20944/preprints201803.0093.v1

Peer-reviewed version available at Sensors 2018, 18, 1236; doi:10.3390/s18041236

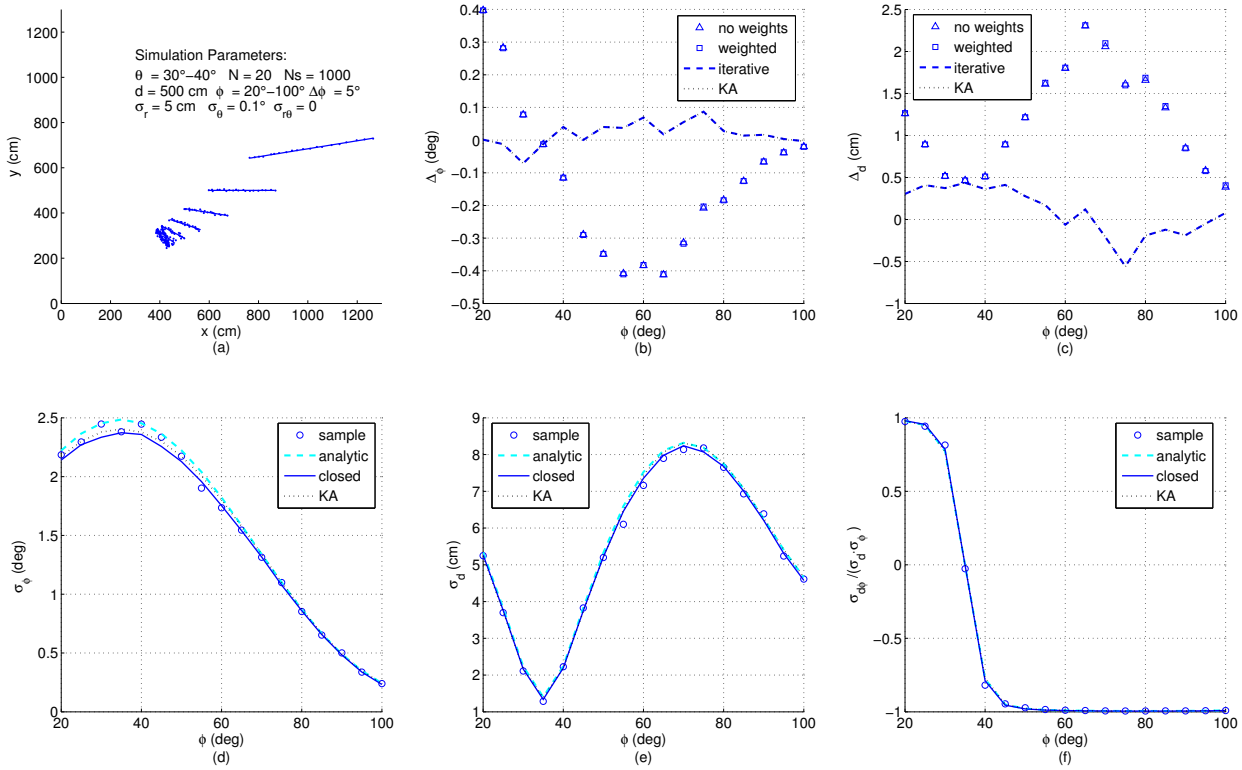

Figure 8. Results from simulated range-bearing scans of short lines superimposing low noise in *r*- and *θ*-direction

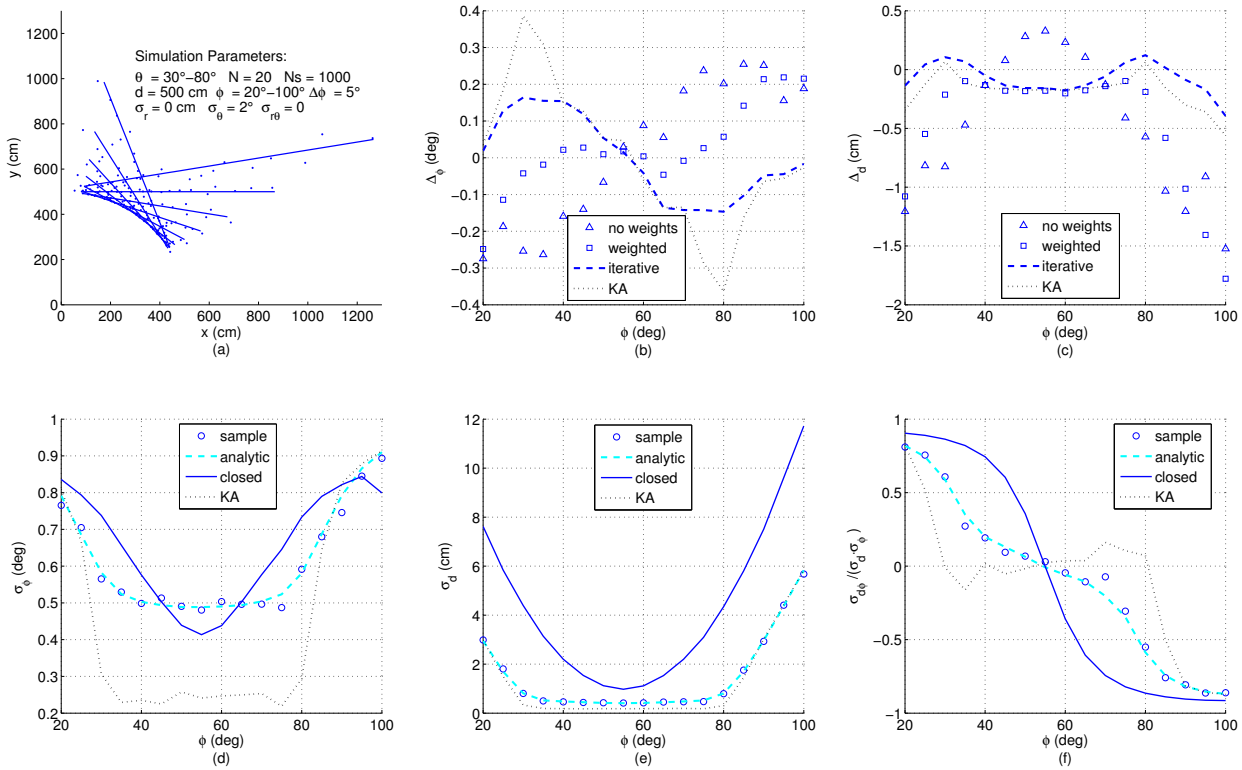

Figure 9. Results from simulated range-bearing scans superimposing high noise only in *θ*-direction

Preprints (www.preprints.org) | NOT PEER-REVIEWED | Posted: 13 March 2018 doi:10.20944/preprints201803.0093.v1

Peer-reviewed version available at Sensors 2018, 18, 1236; doi:10.3390/s18041236

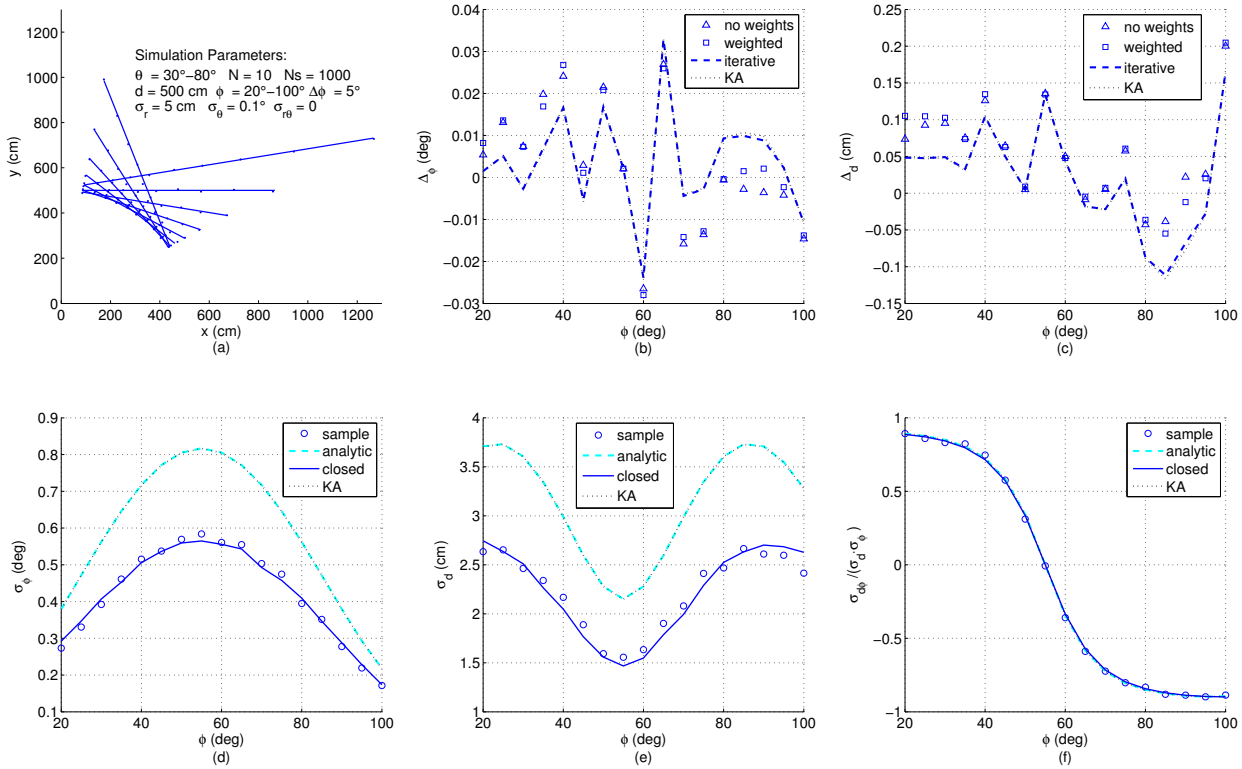

Figure 10. Results from simulated range-bearing scans with a low number of data points and only approximately known noise level of the sensor

than the numerical approaches. All error models however provide still accurate results. Actually, the closed-form model even yields better accuracy than before, since the distances of the data points on the line between adjacent measurement and also $\sigma_{\rho,i}$ are more uniform compared to the simulations with long lines.

In order to check the limits of the models, figure 9 depicts the results when applying large angular noise with $\sigma_\theta = 2°$. In this extreme case also the numerical algorithms show systematic errors dependent on ϕ since the noise of ρ_i can no longer be assumed to be normally distributed. However, according to subfigures (b) and (c) the iterative method as presented in section 2 shows clear benefits in comparison to the KA-algorithm proposed in [32], caused by the more accurate modeling of σ_{ρ_i}.

With respect to the outcome of the noise models in subfigures (d) to (f), now only the analytic algorithm as presented in paragraph 3 still yields reliable results, while the KA-method based on matrix inversion reveals numerical instability. Due to the clear uneven distribution of measurements along the line also the simplified error model in this case shows clear deviations, although at least the order of magnitude is yet correct.

Finally, figure 10 shows typical results, if the sensor noise is not exactly known. In this example, the radial standard deviation was assumed to be 10 cm whereas the exact value, applied when generating the measurements, was only 5 cm. The simulation parameters correspond to those in figure 7, only the number of data points has been reduced to $N = 10$. According to subfigures (b) and (c), now for calculating ϕ and d the numerical methods yield no benefit over the analytical formulas with or without weights. Due to the only approximately known variance, the analytic error model as well as the KA-method in (d) to (f) reveal clear deviations from the reference results. Only the model in closed-form is still accurate, since it does not require any a-priori information regarding sensor noise. In addition, these results prove the bias-free estimation of σ_ρ^2 with (39) also if N is low as depicted in figure 6.

6. Conclusion

In this study the performance of linear regression is evaluated, assuming both coordinates as random variables. It is shown, that especially with range-bearing sensors, frequently used in mobile robotics, a distinct covariance of the noise in x- and y-direction at each measurement point exists. In this case, analytical formulas assuming identical and uncorrelated noise, will only provide accurate line parameters ϕ and d if the detected line segments are sufficiently long and the noise level stays below a certain limit. If this prerequisites are not fulfilled and if the sensor noise is known, numerical algorithms should be applied, which consider the reliability of each measurement point as a function of ϕ. At this, the performance of prior art can be improved by means of modeling the independence of the single data points exactly and by paying attention also to 2nd order effects of the angular noise.

The main focus of this paper is on the derivation of the covariance matrix $\underline{R}_{d\phi}$ of straight lines. This information has crucial impact on the performance of SLAM with line features, since for both, data association and sensor fusing, $\underline{R}_{d\phi}$ must be estimated precisely. For this purpose, first analytical error models are reviewed, which however need exact knowledge of the measurement noise, although in many applications this is not available. In addition, these approaches require high computational effort and do not allow to comprehend the effect of measurement parameters on the resulting accuracy of an estimated straight line. Thus, a new error model in closed form is proposed, just depending on two geometric parameters as well as on the number of points of a line segment. Besides, a single variance must be known, which is determined easily and reliably from the same measurements as used for line fitting. By means of this model the covariance matrix can be estimated fast and exactly. Moreover, it allows to adapt measurement conditions in order to achieve maximum accuracy of detected line features.

Appendix. Analytic derivation of straight line parameters with errors in both coordinates

For the derivation of the perpendicular distance d, the partial derivative of equation (2) with respect to d is taken and set to zero, which directly gives equation (4) using (8), (9) and (10). In order to calculate ϕ, first the partial derivation of (2) with respect to ϕ must be calculated and set to zero, yielding:

$$\frac{1}{N}\sum_{i=1}^{N} s_i \left[x_i y_i \left(\cos^2\phi - \sin^2\phi\right) + \left(y_i^2 - x_i^2\right)\sin\phi\ \cos\phi\right] + \frac{1}{N}\sum_{i=1}^{N} s_i d\left(x_i \sin\phi - y_i \cos\phi\right) = 0 \tag{A1}$$

Now, the distance d can be replaced by (4), and after inserting the definitions of $\bar{x}$, $\bar{y}$, σ_x^2, σ_y^2 and σ_{xy} according to (5) - (9) considering (10) it follows from (A1) after reordering:

$$\sigma_{xy}\left(\cos^2\phi - \sin^2\phi\right) + \sin\phi\cos\phi\left(\sigma_y^2 - \sigma_x^2\right) = 0 \tag{A2}$$

Applying the theorem of *Pythagoras* and the addition theorems of angles, the terms with sine and cosine can be rewritten:

$$\cos^2\phi - \sin^2\phi = 2\cos^2\phi - 1 = \cos 2\phi \tag{A3}$$

$$\sin\phi\cos\phi = \frac{1}{2}\sin 2\phi \tag{A4}$$

Inserting these formulas into (A2), finally yields for ϕ:

$$\phi = \frac{1}{2}\arctan\left(\frac{-2\sigma_{xy}}{\sigma_y^2 - \sigma_x^2}\right) \tag{A5}$$

(A5) calculates ϕ always in the range $-\pi/4 < \phi < \pi/4$, although according to fig. 1 this is only correct if $\sigma_y^2 > \sigma_x^2$, while in the case $\sigma_y^2 < \sigma_x^2$ an angle $\pi/2$ must be added to ϕ. Thus, as general solution (3) should be taken also avoiding a special consideration if σ_y^2 equals σ_x^2.

References

1. Everett, H.R. *Sensors for Mobile Robots*; Number ISBN 978-1568810485, A. K. Peters, 1995.
2. Canny, J. A Computational Approach to Edge Detection. *IEEE Trans. Pattern Analysis and Machine Intelligence* **1986**, *8*, 679–698.
3. Guse, W.; Sommer, V. A New Method for Edge Oriented Image Segmentation. *Picture Coding Symposium, Tokio* **1991**.
4. Gao, Y.; Liu, S.; Atia, M.M.; Noureldin, A. INS/GPS/LiDAR Integrated Navigation System for Urban and Indoor Environments Using Hybrid Scan Matching Algorithm. *Sensors* **2015**, *15*, 23286–23302.
5. Lu, F.; Milios, E. Robot pose estimation in unknown environments by matching 2D range scans. *Journal of Intelligent and Robotic Systems* **1997**, *18*, 249–275.
6. Arras, K.O.; Castellanos, J.A.; Schilt, M.; Siegwart, R. Feature-based multi-hypothesis localization and tracking using geometric constraints. *Robotics and Autonomous Systems* **2003**, *44*, 41–53.
7. Borenstein, J.; Everett, H.R.; Feng, L. *Navigating Mobile Robots, Systems and Techniques*; Number ISBN 978-1568810669, A. K. Peters, 1996.
8. Neira, J.; Tardos, J.D. Data association in stochastic mapping using the joint compatibility test. *IEEE Transactions on Robotics and Automation* **2001**, *17*, 890–897.
9. Durrant-Whyte, H.; Bailey, T. Simultaneous localization and mapping: part I. *IEEE Robotics & Automation Magazine* **2006**, *13*, 99–110.
10. Blanco, J.L.; Gonzalez-Jimenez, J.; Fernandez-Madrigal, J.A. An Alternative to the Mahalanobis Distance for Determining Optimal Correspondences in Data Association. *Transactions on Robotics* **2012**, *28*, 980–986.
11. Wang, H.; Liu, Y.H.; Zhou, D. Adaptive Visual Servoing Using Point and Line Features With an Uncalibrated Eye-in-Hand Camera. *IEEE Transactions on Robotics* **2008**, *24*, 843–857.
12. Choi, Y.H.; Lee, T.K.; Oh, S.Y. A line feature based SLAM with low grade range sensors using geometric constraints and active exploration for mobile robot. *Autonomous Robots* **2008**, *24*, 13–27.
13. Yin, J.; Carlone, L.; Rosa, S.; Anjum, M.L.; Bona, B. Scan Matching for Graph SLAM in Indoor Dynamic Scenarios. *Proceedings of the Twenty-Seventh International Florida Artificial Intelligence Research Society Conference* **2014**, pp. 418–423.
14. Pasteau, F.; Narayanan, V.K.; Babel, M.; Chaumette, F. A visual servoing approach for autonomous corridor following and doorway passing in a wheelchair. *Robotics and Autonomous Systems* **2016**, *75*, 28–40.
15. David, P.; DeMenthon, D.; Duraiswami, R.; Samet, H. Simultaneous pose and correspondence determination using line features. *Proc. of Computer Vision and Pattern Recognition* **2003**, *2*, 424–431.
16. Marchand, É.; Fasquelle, B. Visual Servoing from lines using a planar catadioptric system. *Conf. on Intelligent Robots and Systems (IROS)* **2017**, pp. 2935–2940.
17. Bista, S.R.; Giordano, P.R.; Chaumette, F. Combining Line Segments and Points for Appearance- based Indoor Navigation by Image Based Visual Servoing. *IEEE/RSJ International Conference on Intelligent Robots and Systems (IROS)* **2017**, pp. 2960–2967.
18. Xu, D.; Lu, J.; Wang, P.; Zhang, Z.; Liang, Z. Partially Decoupled Image-Based Visual Servoing Using Different Sensitive Features. *IEEE Transactions on Systems, Man, and Cybernetics: Systems* **2017**, *47*, 2233–2243.
19. Jeong, W.Y.; Lee, K.M. Visual SLAM with Line and Corner Features. Conference on Intelligent Robots and System, IROS. IEEE, 2006.
20. York, D. Least-squares fitting og a straight line. *Can. J. Phys.* **1966**, *44*, 1079–1086.
21. Krane, K.S.; Schecter, L. Regression line analysis. *Am. J. Phys.* **1982**, *50*.
22. Golub, G.; van Loan, C. Ana analysis of the total least squares problem. *SIAM J. Num. Anal.* **1980**, *17*, 883–893.
23. Weisberg, S. *Applied linear regression*, 3rd edition ed.; Number ISBN 0-471-66379-4, John Wiley & Sons, 2005.
24. Draper, N.R.; Smith, H. *Applied Regression Analysis*, 3rd edition ed.; John Wiley & Sons, 1988.
25. Seber, G.A.F.; Lee, A.J. *Linear Regression Analysis*, 2nd edition ed.; Number ISBN 0 471 41540 5, John Wiley & Sons, 2003.

26. Amiri-Simkooeiab, A.R.; Zangeneh-Nejadac, F.; Asgaria, J.; Jazaeri, S. Estimation of straight line parameters with fully correlated coordinates. *Journal of the International Measurement Confederation* **2014**, *48*, 378–386.
27. Krystek, M.; Anton, M. A weighted total least-squares algorithm for fitting a straight line. *Measurement Science and Technology* **2007**, *18*, 3438–3442.
28. Cecchi, G.C. Error analysis of the parameters of a least-squares determined curve when both variables have uncertainties. *Measurement Science and Technology* **1991**, *2*, 1127–1129.
29. Arras, K.O.; Siegwart, R.Y. Feature Extraction and Scene Interpretation for Map-Based Navigation and Map Building. Proc. of SPIE, Mobile Robotics XII, 1997, pp. 42–53.
30. Pfister, S.T.; Kriechbaum, K.L.; S. I. Roumeliotis, J.W.B. A Weighted range sensor matching algorithms for mobile robot displacement estimation. *Proceedings IEEE International Conference on Robotics and Automation* **2002**, *4*.
31. Pfister, A.T.; Roumeliotis, S.I.; Burdick, W. Weighted line fitting algorithms for mobile robot map building and efficient data representation. *Proc. of the 2003 IEEE int. Conf. on Robotics and Automation* **2003**, pp. 1304–1311.
32. Krystek, M.; Anton, M. A least-squares algorithm for fitting data points with mutually correlated coordinates to a straight line. *Measurement Science and Technology* **2011**, *22*, 1–9.
33. Borges, G.A.; Aldon, M.J. A Split-and-Merge Segmentation Algorithm for Line Extraction in 2-D Range Images. *Proceedings. 15th International Conference on Pattern Recognition* **2000**, *4*.
34. Jian, M.; Zhang, C.F.; Yan, F.; Tang, M.Z. A global line extraction algorithm for indoor robot mapping based on noise eliminating via similar triangles rule. *35th Chinese Control Conference (CCC)* **2016**, pp. 6133–6138.
35. J.Illingworth.; J.Kittler. A survey of the hough transform. *Computer Vision, Graphics, and Image Processing* **1988**, *44*, 87–116.
36. Kim, J.; Krishnapuram, R. A Robust Hough Transform Based on Validity. Internat. Conf. on Computational Intelligence. IEEE, 1998, Vol. 2, pp. 1530–1535.
37. Banjanovic-Mehmedovic, L.; Petrovic, I.; Ivanjko, E. Hough Transform based Correction of Mobile Robot Orientation. *Internat. Conf. on Industrial Technology* **2004**, *3*, 1573–1578.
38. Fischler, M.A.; Bolles, R.C. Random Sample Consensus: A Paradigm for Model Fitting with Applications to Image Analysis and Automated Cartography. *Communications of the ACM* **1981**, *25*, 381–395.
39. Liu, Y.; Gu, Y.; Li, J.; Zhang, X. Robust Stereo Visual Odometry Using Improved RANSAC-Based Methods for Mobile Robot Localization. *Sensors* **2017**, *17*, 2339–2357.
40. Nguyen, V.; Martinelli, A.; Tomatis, N.; Siegwart, R. A Comparison of Line Extraction Algorithms using 2D Laser Rangefinder for Indoor Mobile Robotics. Conference on Intelligent Robots and System, IROS. IEEE, 2005.
41. Westfall, P.H. *Understanding Advanced Statistical Methods, chapter 16*; CRC Press, 2013.
42. Dovì, V.G.; Paladino, O.; Reverberi, A.P. Some remarks on the use of the inverse hessian matrix of the likelihood function in the estimation of statistical properties of parameters. *Applied Mathematics Letters* **1991**, *4*, 87–90.
43. Garulli, A.; Giannitrapani, A.; Rossi, A.; Vicino, A. Mobile robot SLAM for line-based environment representation. *Proceedings of the 44th IEEE Conference on Decision and Control* **2005**, pp. 2041–2046.